Stratification in the northern Bering Sea in early summer of 2017 and 2018

Hiromichi Ueno[a,b*], Mizuki Komatsu[a], Zhaoqianyi Ji[c], Ryo Dobashi[a], Miaki Muramatsu[a], Hiroto Abe[a], Keiri Imai[a], Atushi Ooki[a,b] Toru Hirawake[a,b]

a Faculty of Fisheries Sciences/Graduate School of Fisheries Sciences, Hokkaido University, 3-1-1 Minato-cho, Hakodate, 041-8611, Japan

b Arctic Research Center, Hokkaido University, Kita-21 Nishi-11 Kita-ku, Sapporo, Hokkaido, 001-0021, Japan

c College of Marine Ecology and Environment, Shanghai Ocean University, No.999, Huchenghuan Rd, Nanhui New City, Shanghai, P.R. 201306, China

*Corresponding author.

E-mail address: ueno@fish.hokudai.ac.jp (H. Ueno)

Abstract

We investigated spatial and interannual variation in the physical environment in the northern Bering Sea focusing on stratification, which is one factor affecting biological production in Arctic/subarctic regions. In particular, we analyzed in situ data obtained onboard the training ship Oshoro Maru in early summer in 2017 and 2018. We found that stratification in the areas just north of St. Lawrence Island (around 64.5°N and west of 168.5°W) and south/southwest of St. Lawrence Island was significantly weaker in 2018 than in 2017. These results are consistent with the extremely low sea-ice extent present in the winter of 2017/2018, which would have resulted in less freshwater being supplied to the surface layers and a warmer and less saline bottom water. Conversely, stratification was as strong in 2018 as in 2017 in the area close to the Alaska mainland, including the Bering Strait area, suggesting that the Alaskan Coastal Water dominates stratification in this area in early summer. Moreover, we found that the weakly stratified water column in the Bering Strait area stratified quickly shortly after the occurrence of strong northerly winds, likely because of the Ekman transport of warm and low-salinity Alaskan Coastal Water from the east.

Keywords: northern Bering Sea, stratification, interannual variation, in situ data

1. Introduction

The northern Bering Sea, a broad continental shelf region with seasonal sea ice (Fig. 1), is one of the most productive marine ecosystems worldwide (Grebmeier et al., 2012). It has been suggested that this ecosystem is influenced by the timing of sea ice retreat, which manifests as changes in temperature and stratification (Hunt et al., 2011). Historically, the northern Bering Sea has been largely ice-covered for 5–6 months each year; although there has been considerable variability in the timing of ice arrival and retreat, no significant trend in these variables was evident from 1979 to 2014 (Stabeno et al., 2019). However, in the winter of 2017/2018, the winter-maximum areal sea-ice coverage was extremely low (Stabeno and Bell, 2019). Sea ice arrived late owing to warm southerly winds in November, while warm southerlies in February and March prevented southward migration of sea ice (Stabeno and Bell, 2019). The resulting reduction in sea-ice coverage caused very low stratification at mooring site M8 (62.19°N, 174.69°W), located southwest of St. Lawrence Island (SLI); weaker stratification persisted until the summer/fall of 2018 owing to the decrease of cold bottom water and fresh surface water (Stabeno and Bell, 2019). In addition, weak stratification delays in the timing of the spring bloom and a paucity of large copepods were observed in the northern Bering Sea (Duffy-Anderson et al., 2019).

Water in the northern Bering Sea consists of the Alaska Coastal Water (ACW), Bering Shelf Water (BSW), and Anadyr Water (AW) (Coachman et al., 1975; Danielson et al., 2017). The ACW comprises warm, low-salinity, and nutrient-poor water, which is influenced by fresh coastal discharges from Alaskan rivers (Danielson et al., 2017). More than half of the discharge into the Bering Shelf is from the Yukon River (Aagaard et al., 2006), which shows the highest flow in June (Yang et al., 2009). The nutrient distribution in the region surrounding SLI is governed by the high-salinity AW, which upwells onto the Bering Sea shelf from the Bering Slope Current (Kinder et al., 1975; Wang et al., 2009; Cooper et al., 2012). The BSW has similar temperature and salinity to the AW as a result of cycles of freezing, brine rejection, and subsequent summer warming, but lacks the important slope-derived AW nutrient load (Danielson et al., 2017).

Stratification is one of the primary factors affecting biological production in Arctic/subarctic regions (Gargett, 1997, Coyle et al., 2008, Ladd and Stabeno, 2012, Martini et al., 2016). Gargett (1997) proposed an optimum stability window hypothesis, suggesting that there is a range of stability values for which the associated supplies of both nutrients and light are sufficient to stimulate primary production. In this context, the static stability of an oceanic water column has both positive and negative effects on phytoplankton growth and, therefore, on the level of primary production. Ladd et al. (2018) found a significant nonlinear relationship between coccolithophore bloom and summer stratification: coccolithophore blooms were larger during years with either very low or very high stratification in the eastern Bering Sea shelf. In addition, while the blooms usually occurred over the middle shelf (50- to 100-m depth), more of the bloom was located over the shallow (30–50 m) inner shelf when stratification was low. Meanwhile, Coyle et al. (2008) suggested that the optimum stability for production of large zooplankton is relatively weak. In addition, stratification could be broken in the short (several days) timescale by storms, affecting the chlorophyll concentration in the southeastern Bering Sea shelf (Stabeno et al., 2010).

Ladd and Stabeno (2012) defined a stratification index (SI) and studied spatial and temporal variation in the SI for the eastern Bering Sea shelf. They found that both temperature and salinity influence the stratification of this shelf region, with their relative importance varying both spatially and temporally. In the northern middle shelf domain (north of 60°N), salinity stratification is often as important as temperature stratification. Conversely, in the southern middle shelf domain, the influence of temperature dominates stratification during summer, while salinity stratification is also influential in interannual variability. They further demonstrated that September chlorophyll biomass is negatively correlated with August stratification in the southeastern part of the Bearing Sea shelf.

In this study, we investigated spatial and interannual variation in early summer stratification in the northern Bering Sea in 2017 and 2018. In particular, we used the SI modified from Ladd and Stabeno (2012) to clarify the impact of record-breaking low sea-ice extent in the winter of 2017/2018 on stratification in early summer 2018. In the winter of 2016/2017, the period of sea-ice cover in the northern Bering Sea was below the long-term average (Stabeno et al., 2019); accordingly, we have also included data obtained in the early summer of 2013 as an example of moderate sea-ice cover.

2. Data and Methods

We used temperature and salinity data obtained by the training ship Oshoro Maru (Hokkaido University) over the northern Bering Sea during the following periods: July 4–9, 2013; July 9–

22, 2017; and July 2–12, 2018 (Figs. 1 and 2). Temperature and salinity observations by Oshoro-maru were performed with a conductivity-temperature-depth profiler (CTD, Sea-Bird SBE 911plus CTD system with SBE 9plus CTD Unit and SBE 11plus Deck Unit) and expendable CTDs (XCTDs: XCTD-1 and XCTD-4, Tsurumi-Seiki Co., Ltd.). The temperature and salinity at 0–4 dbar were replaced by those at 5 dbar because temperature and salinity data are noisy near the sea surface. We calculated the density of sea water based on the temperature and salinity data and evaluated the SI. The SI of Ladd and Stabeno (2012) (hereafter, SI(LS12)) is defined as potential energy relative to the mixed state (J m^{-2}) and described as follows:

$$SI(LS12) = -\int_{-h}^{0} (\rho - \langle\rho\rangle) gz\, dz; \quad \langle\rho\rangle = \frac{1}{h}\int_{-h}^{0} \rho\, dz \tag{1}$$

where ρ is the density and h is the depth of the water column. Because the depth of the region north of St. Laurence Island is ~50 m, we set h to 50 m, or to the bottom depth where this was shallower than 50 m. In the present study, we discuss spatial variation in stratification; therefore, we divided the SI by depth h to reduce the dependence of h on SI:

$$SI = -\frac{1}{h}\int_{-h}^{0} (\rho - \langle\rho\rangle) gz\, dz; \quad \langle\rho\rangle = \frac{1}{h}\int_{-h}^{0} \rho\, dz \tag{2}$$

where SI is expressed in J m^{-3}. We also calculated the temperature stratification index (SI(T)), that is potential energy due to temperature stratification relative to the mixed state, assuming that the salinity is uniform (= depth-averaged salinity) over the water column in (2). The salinity stratification index (SI(S)) is calculated using depth-averaged temperature. The SI equals 0 when the water column is vertically mixed and increases as the water column stratifies.

For nutrient concentration, we used NO_2^- (nitrite) + NO_3^- (nitrate) concentrations measured according to the colorimetric method using a QuAAtro 2-HR system (BL-tec, Osaka, Japan; Seal Analytical, Norderstedt, Germany) certified with standard reference materials for nutrient analysis (KANSO, standard Lot BT, Osaka, Japan). Seawater samples without filtering were frozen at –65°C in a deep freezer and kept in a freezer at –25°C until the nutrient analysis in the laboratory. We used NCEP-CFSv2 (Saha et al., 2010, https://rda.ucar.edu/datasets/ds094.0/, 2.5° × 2.5°, six-hourly, 1-hour forecast) for mean sea level pressure (hPa) and 10-m wind (m s^{-1}).

3. Results and discussion

Stratification varied spatially and interannually in the northern Bering Sea (Figs. 2a–c). In each year considered, stratification was relatively weak around the Bering Strait and relatively strong south/southwest of SLI. Along 64.5°N, stratification was strong at stations west of 168.5°W and near the coast of Alaska in 2017 but weak at stations west of 168.5°W in 2018.

In 2013, when sea-ice conditions in the northern Bering Sea were moderate (e.g., Fig. 3 of Stabeno et al. (2019)), stratification was weak at stations north of 65°N, moderate near the Alaskan coast, and strong south/southwest of SLI (Fig. 2a). We attribute the strong stratification at stations south/southwest of SLI primarily to salinity stratification east of 174°W and a combination of temperature and salinity stratifications west of 174°W (Figs. 2d and 2g). Our results indicate that surface waters north of 64.5°N and west of 168.5°W were colder and more saline than those at other stations, leading to weak stratification near the Bering Strait (Fig. 3a, 3d, 3g and 3j). South of SLI, we observed near-freezing saline bottom water (Figs. 3d and 3j) known as Winter Water (e.g. Danielson et al., 2017), leading to strong stratification in the area (Fig. 2a). Conversely, we observed warm, low-salinity ACW-type water near the Alaskan coast, especially in the surface layer (Figs. 3a and 3d).

In 2017, when ice arrival and retreat in the northern Bering Sea occurred later and earlier than usual, respectively (Stabeno et al., 2019), the distribution of the SI was similar to that in 2013 (Fig. 2a–b). However, both surface and bottom temperatures were higher in 2017 than in 2013 (Fig. 3a, 3b, 3d and 3e). Along 64.5°N, where observation was not conducted in 2013, stratification was strong west of 168.5°W and east of 167°W, and relatively weak between these longitudes (Fig. 2b). We attribute this distribution primarily to the spatial pattern of surface salinity, which was higher around 168°W (Fig. 3h).

In the early summer of 2018, following the extreme sea-ice conditions of the 2017/2018 winter, stratification was much weaker than that in 2013 and 2017, especially around SLI (Figs. 2a–c). Both temperature and salinity stratification contributed to the weak stratification in 2018, although salinity had a greater impact (Figs. 2d–i). However, the impact of temperature/salinity structure on stratification varied spatially. Along 64.5°N, for example, stratification weakened from 2017 to 2018 west of 168.5°W, whereas no significant differences were observed between these years east of 168.5°W. To understand these regional differences in interannual variation in greater detail, we defined four areas (Areas A, B, C, and D; Figs. 1 and 2a–c) based on the spatial distribution of the SI.

In Area A (south/southwest of SLI), the SI increased from 2013 to 2017 but decreased from 2017 to 2018 (Fig. 4a). We attribute the 2013–2017 increase to large SI(T) caused by high surface temperatures in 2017 and the 2017–2018 remarkable decrease (significant at the 5% significance level) to both SI(S) and SI(T) decrease (primarily SI(S) decrease) (Figs. 4a–h). The surface and bottom salinities were similar in 2018 (Figs. 4b and 4h); accordingly, SI(S) in 2018 was approximately 1/6 of that in 2017 (Fig. 4a). This result is consistent with that of Stabeno and Bell (2019) based on M8 data analysis, who indicated that cold bottom water did not form extensively in this region in the winter of 2017/2018 and that salinity at 30 m and 55 m depths in early summer of 2018 was almost the same as the climatological salinity at 55 m depth, which is ~0.3 higher than the climatological salinity at 30 m. Such anomalous salinity structure was not observed from 2005 to 2017 (Stabeno et al., 2019), illustrating the extreme conditions in 2018.

In Area B (west of 168.5°W along 64.5°N), the SI was approximately one order of magnitude lower in 2018 than in 2017 (Fig. 5a). We attribute this significant change (significant at the 5% significance level) to the large decrease in surface temperature and increase in surface salinity over this period (Figs. 5c and 5e–h). There was little difference in temperature and salinity between the surface and bottom layers in Area B in 2018 (Figs. 5c, 5f and 5h). In Area C (east of 168.5°W along 64.5°N), on the other hand, we observed a weak decrease in average SI between 2017 and 2018 (Fig. 5b); differences between surface and bottom layers in both temperature and salinity decreased in this area over this period (Figs. 5d–h). In Area D (around the Bering Strait), SI, SI(T), and SI(S) were similar for the years 2013, 2017, and 2018 (Fig. 6a). Although surface and bottom temperatures varied interannually, they varied in tandem; therefore, SI(T) did not vary considerably (Figs. 6a–e). This was also true for salinity (Figs. 6 a–b and 6f–h).

Broadly, stratification was similar in 2017 and 2018 in Areas C and D (Figs. 5b and 6a), which lie relatively close to the Alaskan coast. Conversely, significant differences were observed between 2017 and 2018 in Areas A and B (Figs. 4a and 5a), which are farther away from the Alaska mainland. These results suggest that weak stratification, which was induced by the extremely small sea-ice extent during the winter of 2017/2018 (Stabeno and Bell, 2019), persisted until early summer in areas far from Alaska. In contrast, the water column was re-stratified before early summer in areas near Alaska. These phenomena were evident in the temperature and salinity cross-sections along 64.5°N (Fig. 5e–j). In the western part of this section, the water column was broadly uniform in 2018, particularly in salinity and nutrient concentration, while temperature and salinity stratification was observed in 2017. Conversely, in the eastern part of this section, warm, low-salinity, and low-nutrient water was observed in both 2017 and 2018, particularly near the eastern edge of the section. This warm, low-salinity, and low-nutrient surface water with temperature > 7°C and salinity < 32 is regarded as the ACW, which is influenced by fresh coastal discharges from Alaskan rivers (Danielson et al., 2017).

Figures 2–6 suggest that the extreme low sea-ice conditions of the 2017/2018 winter had an impact on stratification in early summer in the northern Bering Sea, especially in the western part, where the influence of the ACW is limited. However, data obtained around the end of the period of observation in 2018 suggest that in addition to interannual variations in sea-ice conditions, synoptic-scale wind conditions affect stratification in the northern Bering Sea and southern Chukchi Sea. Figure 7a–f shows the temperature/salinity cross-sections and SI along ~169°W before (left) and after (right) the passage of the low-pressure area shown in Fig. 7g and 7h. These results indicate that the water column was mostly uniform in terms of salinity but exhibited very weak temperature stratification before the passage of the low-pressure area (Fig. 7e). Strong stratification, particularly of salinity, was formed south of 66.5°N several days later, after the passage of the low-pressure area (Fig. 7f). During the passage of the low-pressure area, a strong northerly wind was observed for four days (July 08–12) around the Bering Strait (Fig. 7h). Because this time scale (four days) is longer than inertial period in this region (< 1 day), this wind would have resulted in westward Ekman transport, transporting low-salinity and warm water influenced by the ACW from the Alaskan coastal area. The low-salinity and warm layer was thin (< 5 m) in the area except around 65.5°N; therefore, low-salinity and warm surface waters from the northeastern area of the Bering Strait (as indicated e.g. Danielson et al. (2017)) might also contribute to the quick stratification in this area due to south-southwestward (Madsen, 1977) to southwestward surface Ekman drift. Precipitation due to the passage of a low-pressure area also would contribute to the decrease of surface salinity, but surface warming cannot be explained by the strong northerly wind, supporting the hypothesis that stratification after the passage of low-pressure was primarily due to Ekman transport. In the area north of 66.5°N, stratification was weak even after the passage of the low-pressure area (Fig 7f). It is difficult to constrain the impact of the passage of low-pressure conditions in this area because observations were not obtained from the period before this event. However, the lack of warm, low-salinity surface water observed in the area north of 66.5°N could be attributed to the distance of this area from the Alaskan coast.

4. Conclusions

We investigated the impact of extreme sea-ice conditions in the winter of 2017/2018 on stratification in early summer 2018 in the northern Bering Sea, comparing data obtained in July 2018 with those obtained in July 2013 and July 2017. We found that stratification was significantly weaker in 2018 than in 2017 in the areas just north of SLI (around 64.5°N and west of 168.5°W) and south/southwest of SLI. These results are consistent with the extremely low sea-ice extent observed in the winter of 2017/2018, which would have resulted in less freshwater being supplied to surface layers and warmer and less saline bottom water (Stabeno and Bell, 2019). Conversely, in the area near the Alaska mainland, including the Bering Strait region, stratification was as strong in 2018 as in 2017. The warm and low-salinity ACW was observed in this area, forming stratification near Alaska. Broadly, extreme sea-ice conditions in the winter of 2017/2018 had an impact on stratification in the northern Bering Sea, especially in its western part, where the influence of the ACW was considered to be limited.

In addition to interannual variations, a rapid change in stratification (over several days) was observed around the Bering Strait in July 2018. At this time, a low-pressure area passed over the Bering Strait and a strong northerly wind blew over the area for 4 days. The water column had been weakly stratified before the passage of this low-pressure area but became stratified after its passage, particularly in terms of salinity. We suggest that westward Ekman transport due to the northerly wind brought warm and low-salinity ACW from the Alaskan coastal area to the observation area. However, we have not yet clarified how long the strong stratification caused by this northerly wind persisted.

Acknowledgments

The authors thank the officers and crew of the training ship Oshoro Maru. The authors also thank S. Okkonen and an anonymous reviewer for their helpful comments. This study was supported by the Green Network of Excellence (GRENE) Arctic Climate Change Research Project, the Arctic Challenge for Sustainability (ArCS) Project, and a KAKENHI Grant-in-Aid for Scientific Research(C) (Grant Number 18K03736), all of which were funded by the Ministry of Education, Culture, Sports, Science and Technology of Japan.

References

Aagaard, K. Weingartner, T.J., Danielson, S.L., Woodgate, R.A., Johnson, G.C., Whitledge T.E, 2006, Some controls on flow and salinity in Bering Strait, Geophys. Res. Lett., 33, L19602

Coachman, L.K., Aagaard, K., Tripp, R.B., 1975. Bering Strait: The Regional Physical Oceanography. University of Washington Press, Seattle.

Cooper, L.W., Janout, M., Frey, K.E., Pirtle-Levy, R., Guarinello, M., Grebmeier, J.M., Lovvorn, J.R., 2012. The relationship between sea ice break-up, water mass variation, chlorophyll biomass, and sedimentation in the northern Bering Sea. Deep Sea Res. II 71–76, 5–15. https://doi.org/10.1016/j.dsr2.2012.02.002.

Coyle, K.O., Pinchuk, A.I., Eisner, L.B., Napp, J.M., 2008. Zooplankton species composition, abundance and biomass on the Eastern Bering Sea shelf during summer: the potential role of water-column stability and nutrients in structuring the zooplankton community. Deep-Sea Res. II 55, 1775–1791. doi:10.1016/j.dsr2.2008.04.029.

Danielson, S., Eisner, L., Ladd, C., Mordy, C., Sousa, L., Weingartner, T., 2017. A comparison between late summer 2012 and 2013 water masses, macronutrients, and phytoplankton standing crops in the northern Bering and Chukchi Seas. Deep Sea Res. II 135, 7–26.

Duffy-Anderson, J.T., Stabeno, P., Andrews, A.G., III, Cieciel, K., Deary, A., Farley, E., Fugate, C., Harpold C., Heintz, R., Kimmel, D., Kuletz, K., Lamb, J., Paquin, M., Porter, S., Rogers, L., Spear, A., Yasumiishi, E., 2019. Responses of the northern Bering Sea and southeastern Bering

Sea pelagic ecosystems following record-breaking low winter sea ice. Geophysical Research Letters, 46, 9833–9842. https://doi.org/ 10.1029/2019GL083396

Gargett, A.E., 1997. The optimal stability ‘window’: a mechanism underlying decadal fluctuations in North Pacific salmon stocks? Fish. Oceanogr. 6, 109–117.

Grebmeier, J.M., 2012. Shifting patterns of life in the Pacific Arctic and sub-arctic seas. Ann. Rev. Mar. Sci. 4, 63–78. https://doi.org/10.1146/annurev-marine-120710- 100926.

Hunt, G.L., Coyle, K.O., Eisner, L.B., Farley, E.V., Heintz, R.A., Mueter, F., Napp, J.M., Overland, J.E., Ressler, P.H., Salo, S., Stabeno, P., 2011. Climate impacts on eastern Bering Sea food webs: a synthesis of new data and an assessment of the Oscillating Control Hypothesis. ICES J. Mar. Sci., doi:10.1093/icesjms/fsr036.

Kinder, T.H., Coachman, L.K., Galt, J.A., 1975. The Bering slope current system. J. Phys. Oceanogr.5(4),231–244.

Ladd, C., Stabeno, P.J., 2012. Stratification on the Eastern Bering Sea shelf revisited. Deep Sea Res. Part II, 65, 72–83.

Ladd, C., Eisner, L.B., Salo, S.A., Mordy, C.W., Iglesias-Rodriguez, M.D., 2018. Spatial and temporal variability of coccolithophore blooms in the eastern Bering Sea. Journal of Geophysical Research: Oceans, 123, 9119–9136. https://doi.org/10.1029/2018JC014302

Madsen, OS., 1977, A realistic model of the wind-induced Ekman boundary layer, J. Phys. Oceanogr., 7(2), 248-255

Saha, S., Moorthi, S., Pan, H.-L., Wu, X., Wang, J., Nadiga, S., Tripp, P., Kistler, R., Woollen, J., Behringer, D., Liu, H., Stokes, D., Grumbine, R., Gayno, G., Wang, J., Hou, Y.-T., Chuang, H.-Y., Juang, H.-M.H., Sela, J., Iredell, M., Treadon, R., Kleist, D., Van Delst, P., Keyser, D., Derber, J., Ek, M., Meng, J., Wei, H., Yang, R., Lord, S., Van Den Dool, H., Kumar, A., Wang, W., Long, C., Chelliah, M., Xue, Y., Huang, B., Schemm, J.-K., Ebisuzaki, W., Lin, R., Xie, P., Chen, M., Zhou, S., Higgins, W., Zou, C.- Z., Liu, Q., Chen, Y., Han, Y., Cucurull, L., Reynolds, R.W., Rutledge, G., Goldberg, M., 2010. The NCEP climate forecast system reanalysis. Bull. Am. Meteorol. Soc. 91, 1015–1057. http://dx.doi.org/10.1175/2010BAMS3001.1.

Stabeno, P.J., Napp, J., Mordy, C., Whitledge, T., 2010. Factors influencing physical structure and lower trophic levels of the eastern Bering Sea shelf in 2005: sea ice, tides and winds. Prog. Oceanogr. 85 (3–4), 180–196. https://doi.org/10.1016/j. pocean.2010.02.010.

Stabeno, P. J., Bell, S.W., 2019. Extreme conditions in the Bering Sea (2017–2018): Record-breaking low sea-ice extent. Geophysical Research Letters, 46, 8952–8959. https://doi.org/10.1029/2019GL083816

Stabeno, P.J., Bell, S.W., Bond, N.A., Kimmel, D.G., Mordy, C.W., Sullivan, M.E., 2019. Distributed biological observatory region 1: physics, chemistry and plankton in the northern Bering sea. Deep Sea Res. Part II Top. Stud. Oceanogr. 162, 8–21.

Wang, J., Hu, H., Mizobata, K., Saitoh, S., 2009. Seasonal variations of sea ice and ocean circulation in the Bering Sea: a model-data fusion study. J. Geophys. Res. 14, C02011.

Yang, D., Zhao, Y., Armstrong, R., Robinson, D., 2009. Yukon River streamflow response to seasonal snow cover changes. Hydrological Processes, 23(1), 109– 121. https://doi-org.ezoris.lib.hokudai.ac.jp/10.1002/hyp.7216

Figure Captions

Fig. 1. Bottom topography (m) of the northern Bering Sea (colors and contours). Black, blue, and red dots indicate the locations of CTD observations by the training ship Oshoro Maru during the following periods, respectively: July 4–9, 2013; July 9–22, 2017; and July 2–12, 2018. Red triangles with black edge are the same as red dots but for XCTD observations in July 2018. The locations of Areas A–D and mooring site M8 are also shown in the figure.

Fig. 2. (a–c) stratification index (SI), (d–f) temperature stratification index (SI(T)), and (g–i) salinity stratification index (SI(S)) (colored dots) for the following periods: July 4–9, 2013 (a, d, g); July 9–22, 2017 (b, e, h); and July 2–8, 2018 (c, f, i) (J m^{-3}). Boxes A, B, C, and D indicate Areas A, B, C, and D, used to evaluate average values for the area.

Fig. 3. (a–c) Surface temperature (°C), (d–f) bottom temperature (°C), (g–i) surface salinity, and (j–l) bottom salinity (colored dots) for the following periods: July 4–9, 2013 (a, d, g, j); July 9–

22, 2017 (b, e, h, k); and July 2–8, 2018 (c, f, i, l). Surface temperature and salinity are averaged between 0 and 10 dbar. Bottom temperature and salinity are averaged between the deepest depth used for the SI calculation and the depth 10 m above it.

Fig. 4. (a) Interannual variation in stratification index (SI: black dots, error bars indicate ±1 standard deviation), evaluated from density stratification, temperature stratification index (SI(T): blue bars), and salinity stratification index (SI(S): orange bars) (J m^{-3}), (b) surface (red) and bottom (blue) temperature (solid lines: °C) and salinity (broken lines) averaged from data plotted in Figs. 2 and 3 within Area A. The definitions of surface and bottom temperature/salinity are as in Fig. 3. (c–e) temperature (°C) and (f–h) salinity cross-sections in Area A in 2013 (c, f), 2017 (d, g) and 2018 (e, h).

Fig. 5. Interannual variation in (a–b) SI, SI(T) and SI(S) (J m^{-3}), and (c–d) surface/bottom temperature (°C) and salinity averaged in Area B (a, c) and Area C (b, d). Longitudinal (e–f) temperature (°C), (g–h) salinity and (i–j) nutrient concentration (NO_2^- + NO_3^-, μmol L^{-1}) cross-sections along 64.5°N in July 2017 and July 2018. Blue diamonds in (i) and (j) indicate that nutrient concentrations were below lower limit of quantification (0.1 μmol L^{-1}).

Fig. 6. Interannual variation in (a) SI, SI(T) and SI(S) (J m^{-3}), and (b) surface/bottom temperature (°C) and salinity averaged in Area D. Latitudinal (c–e) temperature (°C) and (f–h) salinity cross-sections along ~169°W. Values in 2018 were obtained during July 5–8, 2018 (before passage of low-pressure area).

Fig. 7. (a–b)Temperature (°C) and (c–d) salinity cross-sections, and (e–f) SI, SI(S), and SI(T) along ~169°W during July 5–8, 2018 (before passage of low-pressure area (a, c, e)), and during July 10–12, 2018 (after passage of low-pressure area (b, d, f)). Negative SI(S) indicates that the water column is unstable in salinity. (g) Distribution of 10-m wind (vectors, m s^{-1}) and surface pressure (color, hPa) at 01:00 (UTC) on July 9, 2018 and (h) time series of 10-m wind vectors over the period July 1–14 2018 at 168.75°W and 66.25°N.

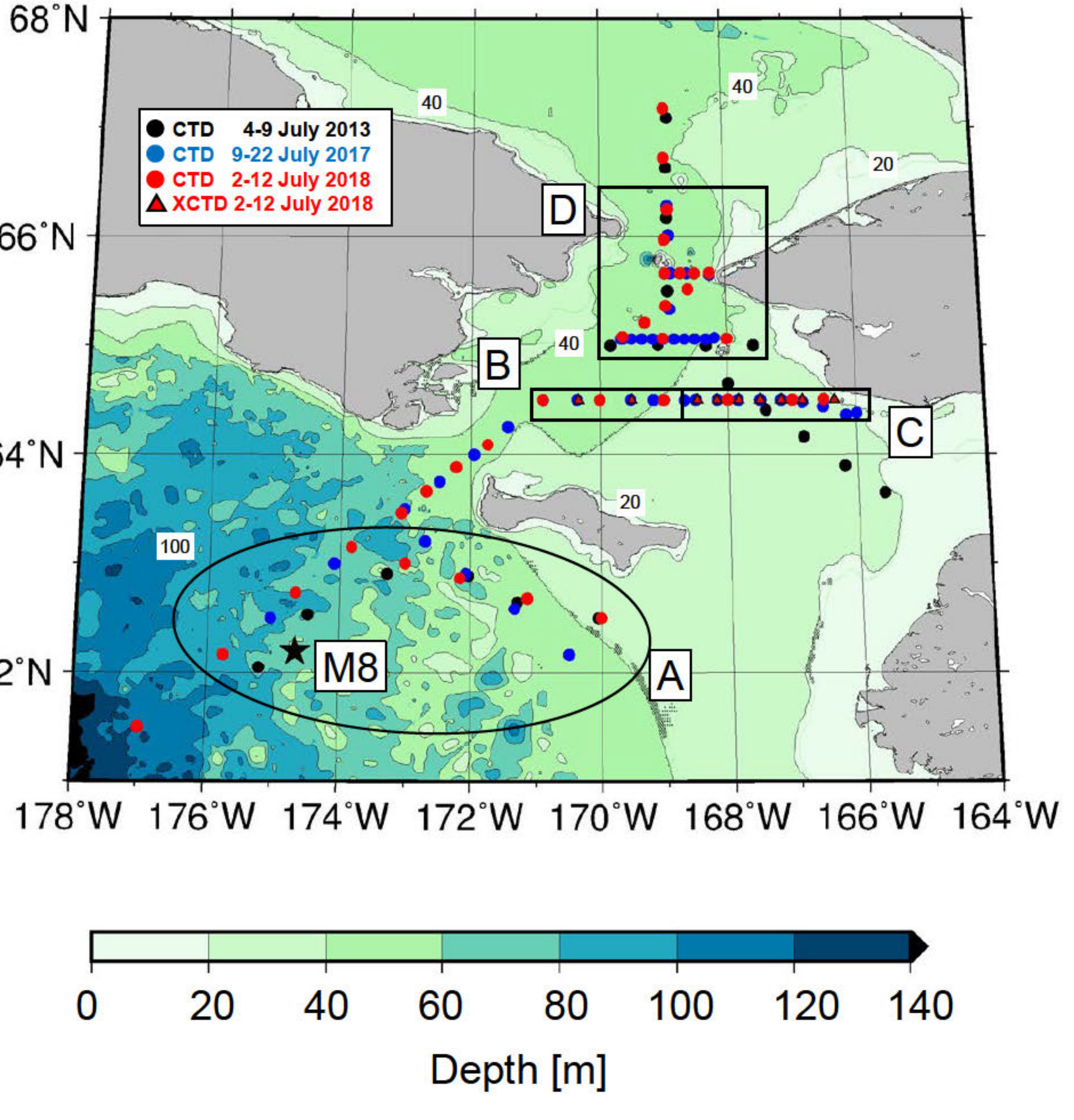

Fig. 1. Bottom topography (m) of the northern Bering Sea (colors and contours). Black, blue, and red dots indicate the locations of CTD observations by the training ship Oshoro Maru during the following periods, respectively: July 4–9, 2013; July 9–22, 2017; and July 2–12, 2018. Red triangles with black edge are the same as red dots but for XCTD observations in July 2018. The locations of Areas A–D and mooring site M8 are also shown in the figure.

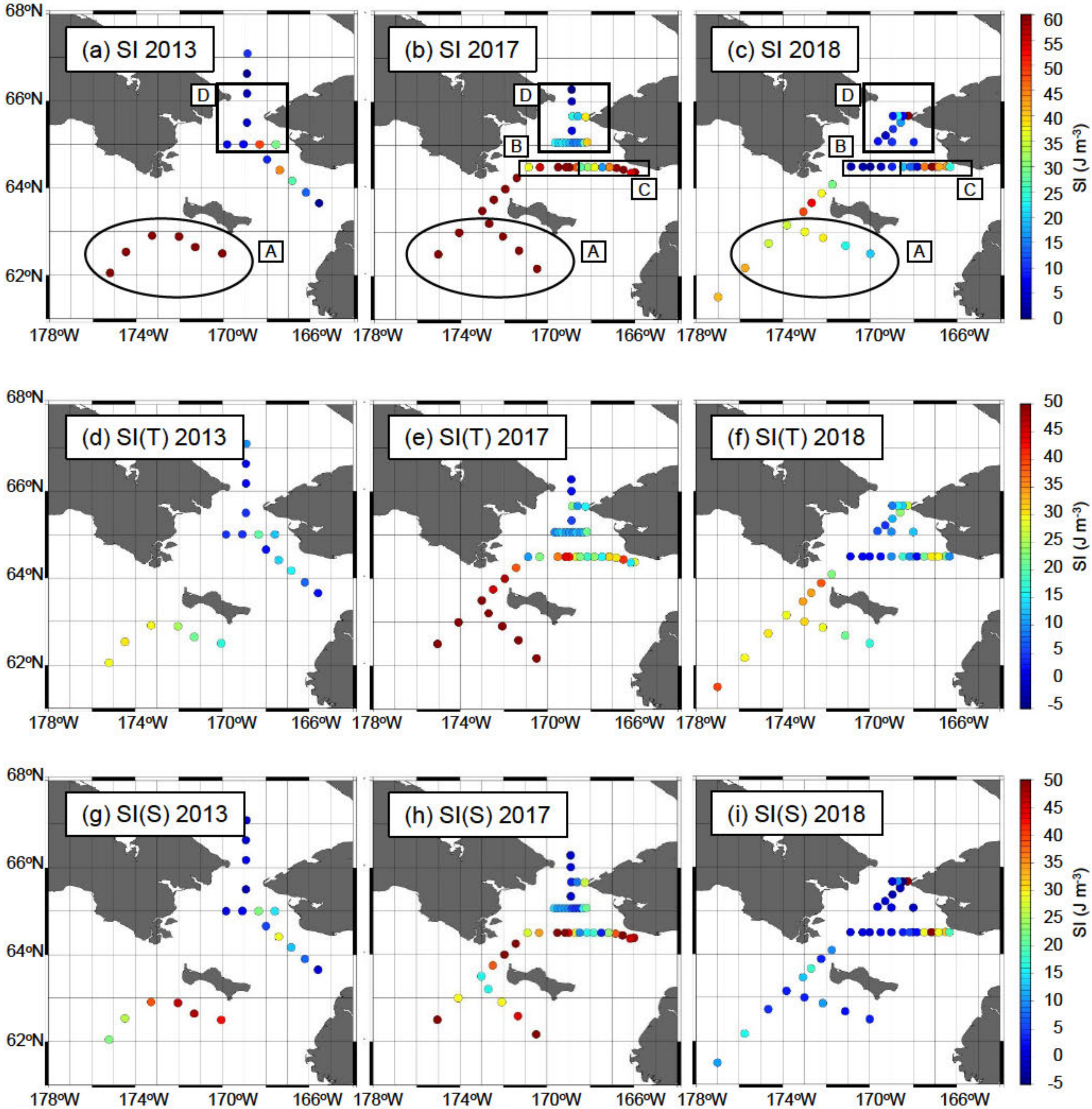

Fig. 2. (a–c) stratification index (SI), (d–f) temperature stratification index (SI(T)), and (g–i) salinity stratification index (SI(S)) (colored dots) for the following periods: July 4–9, 2013 (a, d, g); July 9–22, 2017 (b, e, h); and July 2–8, 2018 (c, f, i) (J m^{-3}). Boxes A, B, C, and D indicate Areas A, B, C, and D, used to evaluate average values for the area.

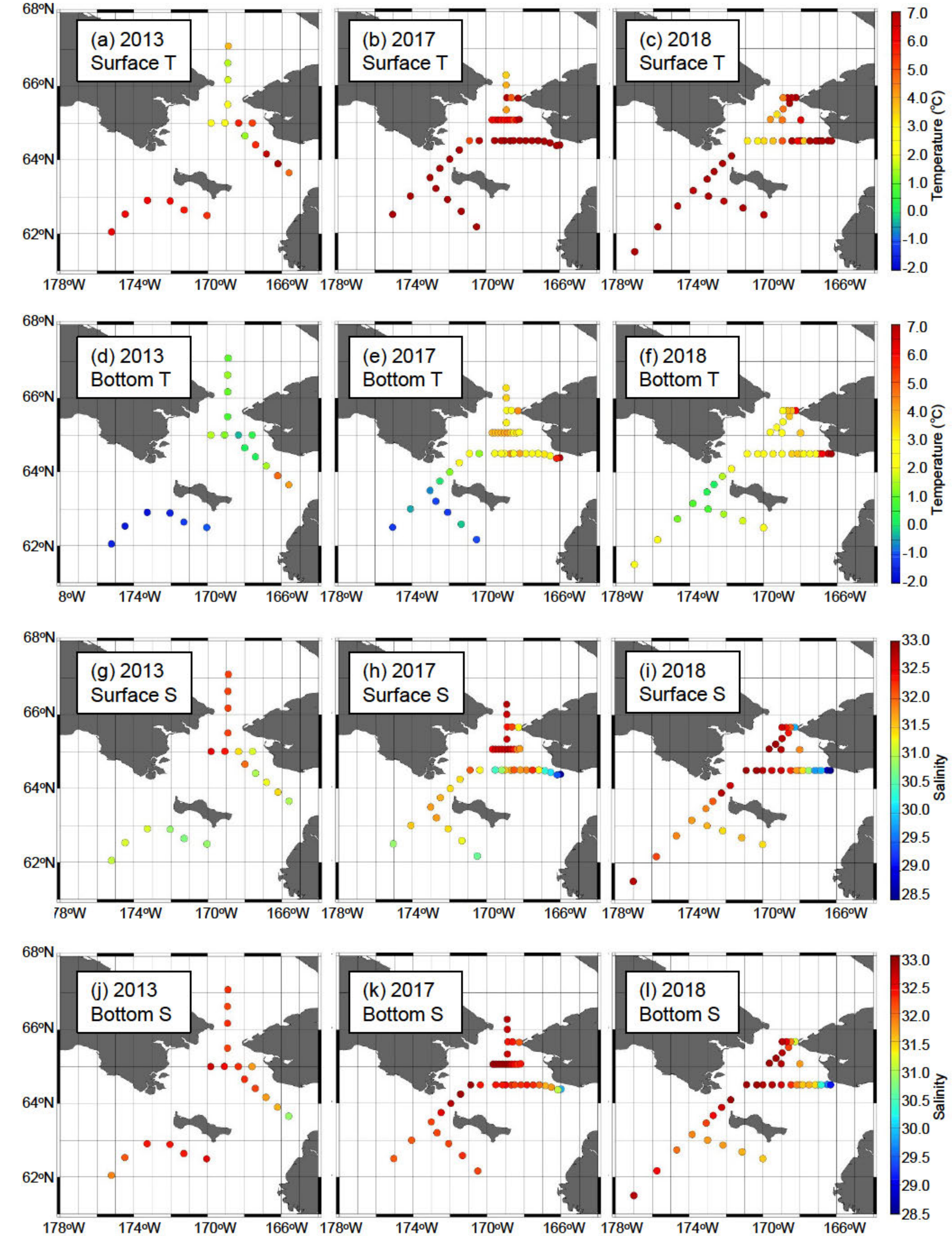

Fig. 3. (a–c) Surface temperature (ºC), (d–f) bottom temperature (ºC), (g–i) surface salinity, and (j–l) bottom salinity (colored dots) for the following periods: July 4–9, 2013 (a, d, g, j); July 9–22, 2017 (b, e, h, k); and July 2–8, 2018 (c, f, i, l). Surface temperature and salinity are averaged between 0 and 10 dbar. Bottom temperature and salinity are averaged between the deepest depth used for the SI calculation and the depth 10 m above it.

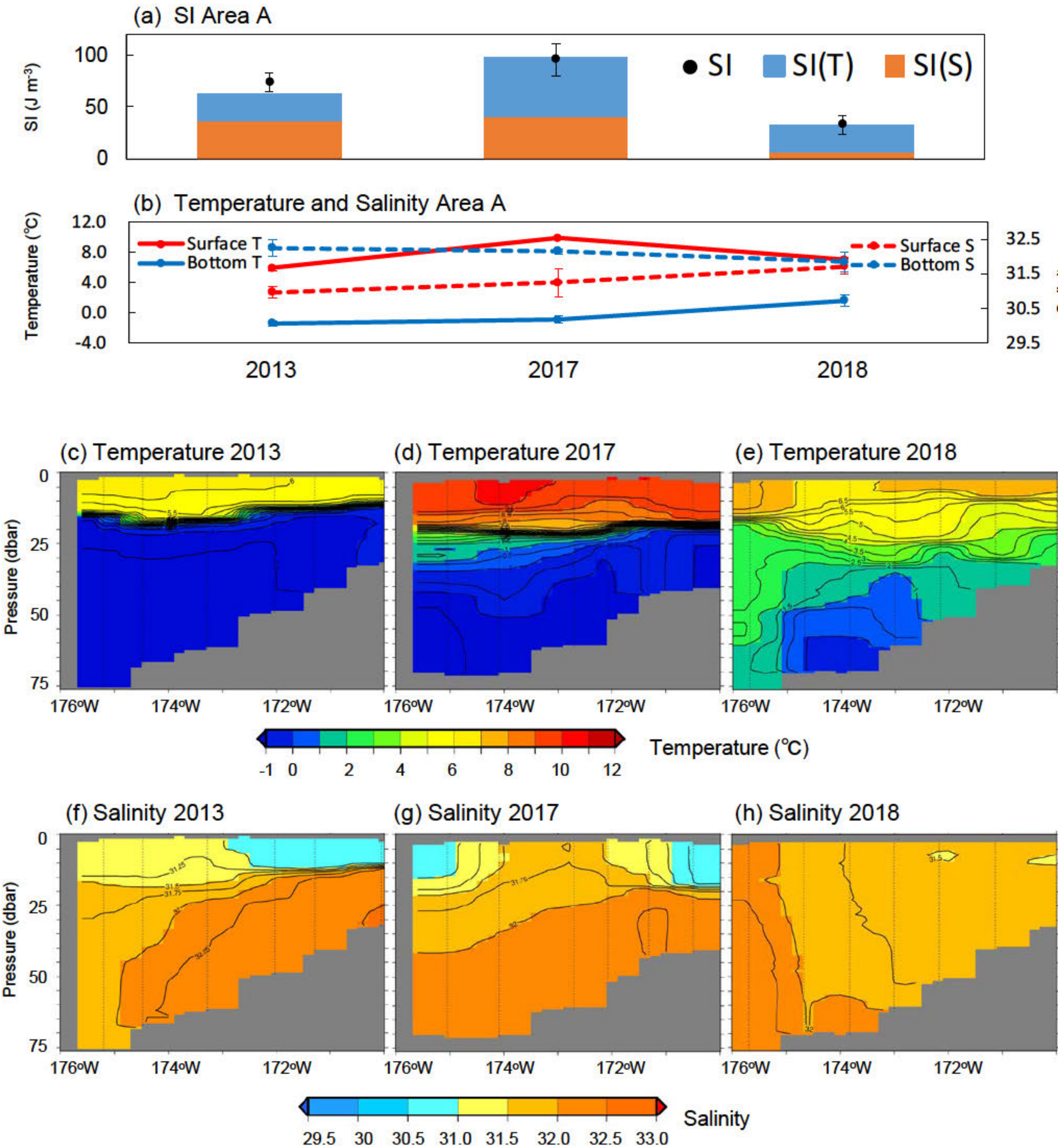

Fig. 4. (a) Interannual variation in stratification index (SI: black dots, error bars indicate ±1 standard deviation), evaluated from density stratification, temperature stratification index (SI(T): blue bars), and salinity stratification index (SI(S): orange bars) (J m-3), (b) surface (red) and bottom (blue) temperature (solid lines: °C) and salinity (broken lines) averaged from data plotted in Figs. 2 and 3 within Area A. The definitions of surface and bottom temperature/salinity are as in Fig. 3. (c–e) temperature (°C) and (f–h) salinity cross-sections in Area A in 2013 (c, f), 2017 (d, g) and 2018 (e, h).

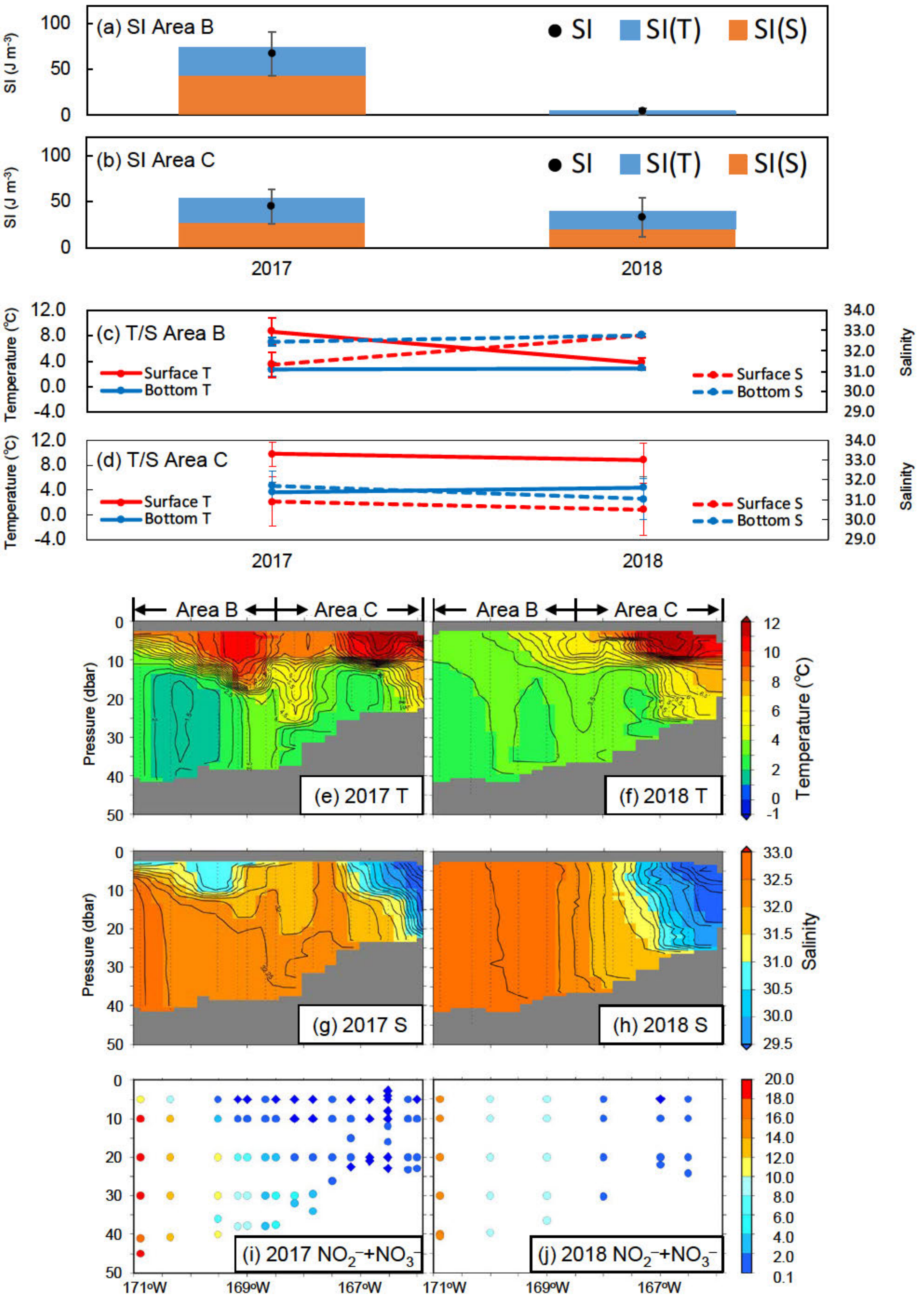

Fig. 5. Interannual variation in (a–b) SI, SI(T) and SI(S) (J m^{-3}), and (c–d) surface/bottom temperature (°C) and salinity averaged in Area B (a, c) and Area C (b, d). Longitudinal (e–f) temperature (°C), (g–h) salinity and (i–j) nutrient concentration (NO2– + NO3–, µmol L^{-1}) cross-sections along 64.5°N in July 2017 and July 2018. Blue diamonds in (i) and (j) indicate that nutrient concentrations were below lower limit of quantification (0.1 µmol L^{-1}).

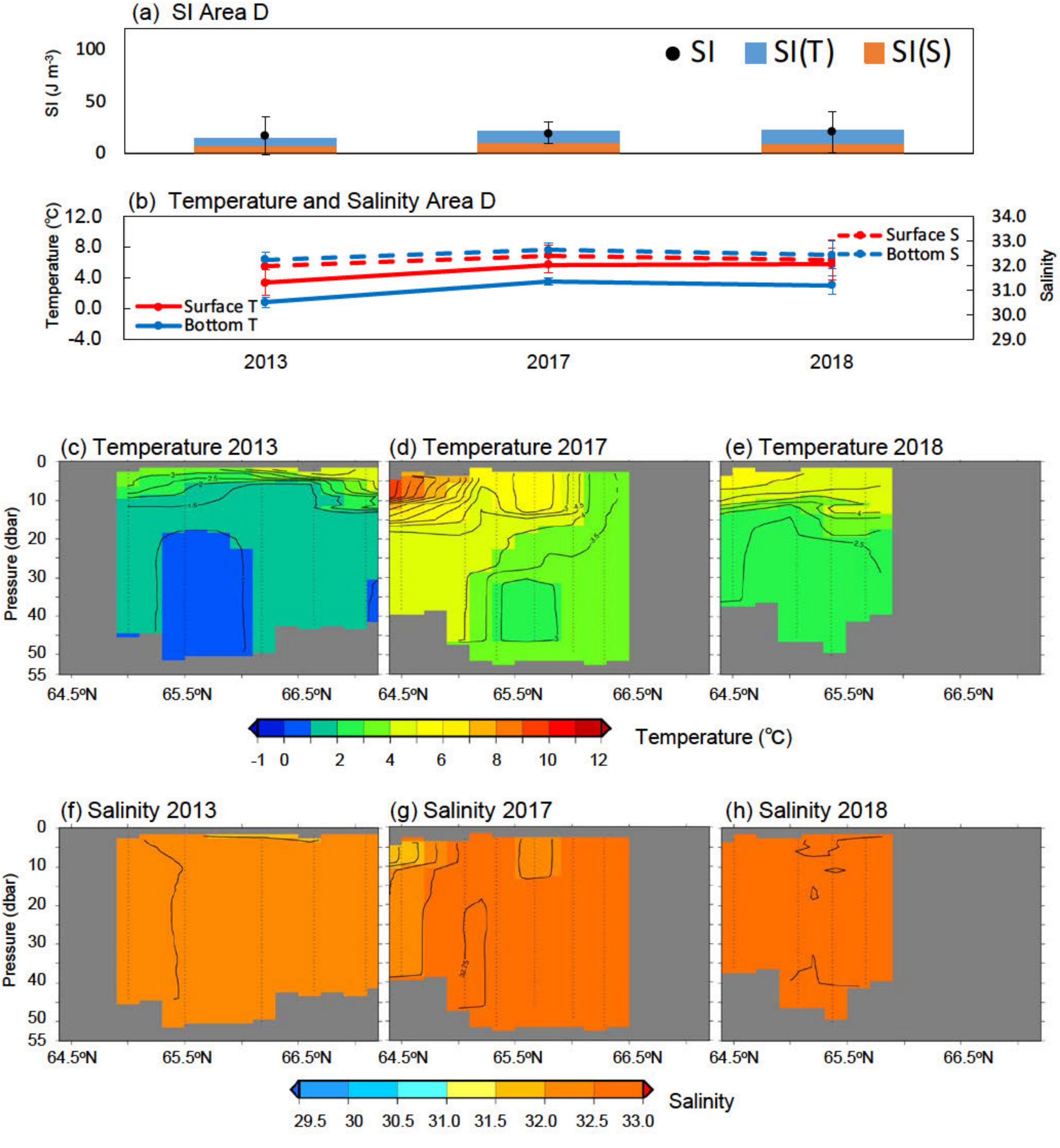

Fig. 6. Interannual variation in (a) SI, SI(T) and SI(S) (J m^{-3}), and (b) surface/bottom temperature (°C) and salinity averaged in Area D. Latitudinal (c–e) temperature (°C) and (f–h) salinity cross-sections along ~169°W. Values in 2018 were obtained during July 5–8, 2018 (before passage of low-pressure area).

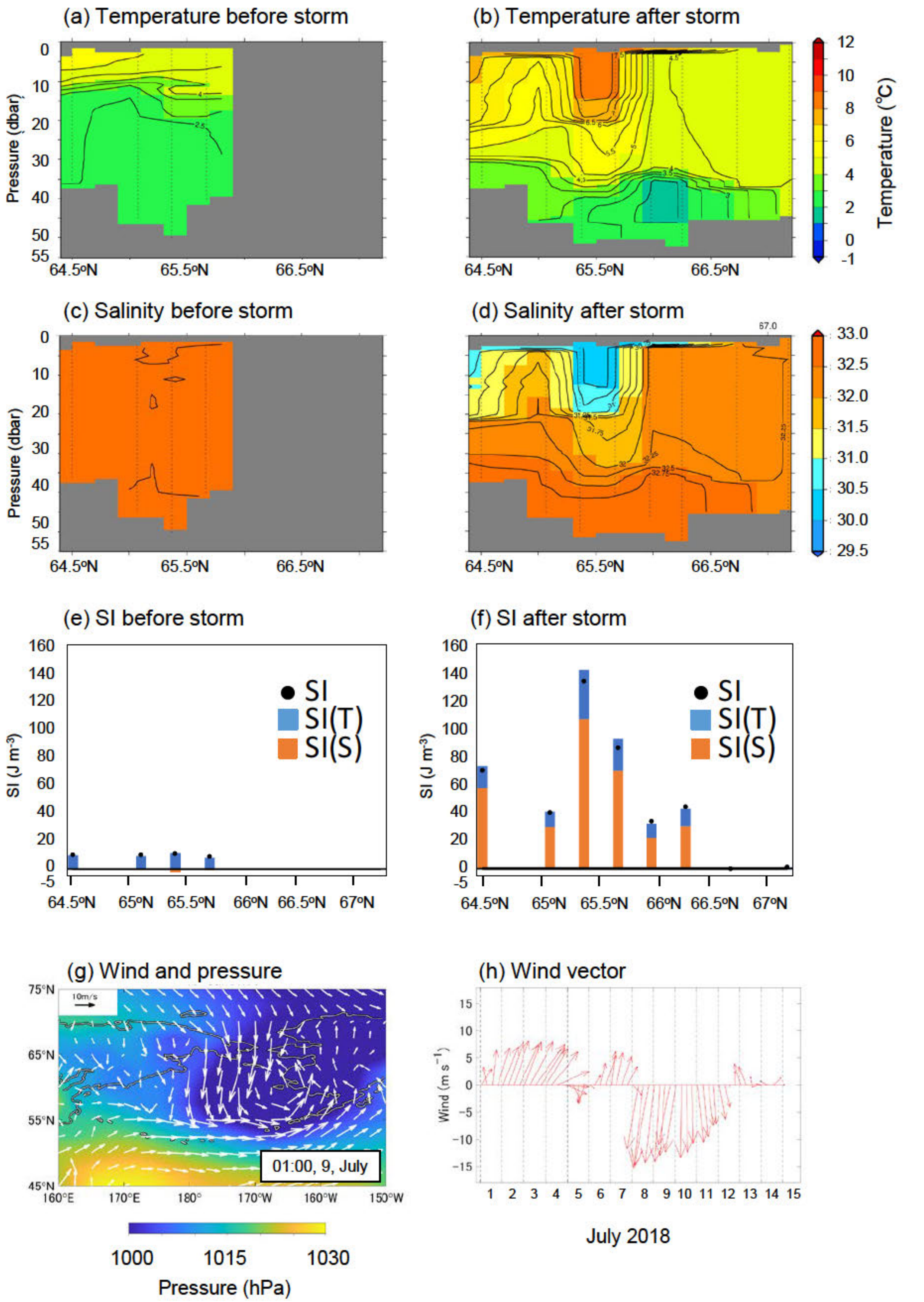

Fig. 7. (a, b)Temperature (°C) and (c, d) salinity cross-sections, and (e, f) SI, SI(S), and SI(T) along ~169°W during July 5–8, 2018 (before passage of low-pressure area (a, c, e)), and during July 10–12, 2018 (after passage of low-pressure area (b, d, f)). Negative SI(S) indicates that the water column is unstable in salinity. (g) Distribution of 10-m wind (vectors, m s^{-1}) and surface pressure (color, hPa) at 01:00 (UTC) on July 9, 2018 and (h) time series of 10-m wind vectors over the period July 1–14 2018 at 168.75°W and 66.25°N.